NOTE

Compositional and morphological properties of platinum-iridium electrodeposited on carbon fiber microelectrodes

Journal of Neural Engineering

RECEIVED
27 February 2021

REVISED
20 August 2021

ACCEPTED FOR PUBLICATION
24 August 2021

PUBLISHED
13 September 2021

NOTE

Compositional and morphological properties of platinum-iridium electrodeposited on carbon fiber microelectrodes

Elena della Valle[1,3,*], **Elissa J Welle**[1,3], **Cynthia A Chestek**[1,3] and **James D Weiland**[1,2,3]

[1] Biomedical Engineering Department, University of Michigan, Ann Arbor, MI, United States of America
[2] Department of Ophthalmology and Visual Sciences, University of Michigan Kellogg Eye Center, Ann Arbor, MI, United States of America
[3] Biointerfaces Institute, University of Michigan, Ann Arbor, MI, United States of America
[*] Author to whom any correspondence should be addressed.

E-mail: eldellav@umich.edu

Keywords: neural interfaces, carbon fiber microelectrodes, electrode coating, platinum-iridium electrochemical deposition, electron microscopy

Abstract

Objective. Neural interfaces based on carbon fiber (CF) electrodes have demonstrated key positive attributes such as minimal foreign body response and mechanical strength to self-insert in brain tissue. However, carbon does not form a low impedance electrode interface with neural tissue. Electrodeposited platinum iridium (PtIr) has been used to improve electrode interface properties for metallic bioelectrodes. *Approach*. In this study, a PtIr electrodeposition process has been performed on CF microelectrode arrays to improve the interfacial properties of these arrays. We study the film morphology and composition as well as electrode durability and impedance. *Results*. A PtIr coating with a composition of 70% Pt, 30% Ir and a thickness of ∼400 nm was observed. Pt and Ir were evenly distributed within the film. Impedance was decreased by 89% @ 1 kHz. Accelerated soak testing in a heated ($T = 50$ °C) saline solution showed impedance increase (@ 1 kHz) of ∼12% after 36 days (89 equivalent) of soaking.

1. Introduction

Neural electrodes are a proven technology for recording and stimulating neuronal activity in a variety of clinical and biomedical research applications. Clinical treatments using neural electrodes include brain stimulation [1–5] to treat movement disorders and epilepsy [6–9], cochlear implants [10, 11] to restore auditory function, retinal prostheses [12, 13] to provide visual sensation [14, 15] and spinal cord stimulation for pain [16]. Neuroscience research also benefits from increasingly sophisticated systems for recording and stimulation in 1000 s of distinct locations in the brain [17]. Pioneering work in human brain-machine interfaces utilize arrays of many (in the 100 s) microelectrodes to form a parallel, functional connection with individual cortical neurons [18, 19].

Electrode materials are a critical part of neural interfaces [20]. Neural stimulation requires specific capability to transfer charge efficiently. Examples of materials used for neural stimulation include sputtered iridium oxide [21, 22], titanium nitride [23], and platinum grey [24]. While neural recording is possible with many materials (e.g. carbon, tungsten), high performance materials, like those used for stimulation, also benefit neural recording by decreasing noise. Electrodeposited platinum-iridium (PtIr) is a high performance material that has been evaluated for neural stimulation [25, 26] and recording [27]. In this report, we provide the first detailed materials analysis of electrodeposited PtIr. Prior works have reported the relative percentage of Pt and Ir in the material [26, 27], but the distribution of the Pt and Ir within the film was not known until our study. Recently, Sarno *et al* [28] analyzed the composition of PtIr nanoalloy formed by surfactant free, ethylene glycol mediated synthesis. By means of scanning electron microscopy (SEM), transmission electron microscopy (TEM), energy dispersive x-ray maps and x-ray diffraction spectra techniques, they found that higher pressures and the presence of hydrogen lead to a homogeneous and well distributed PtIr nanoalloy. Others have used similar materials analysis techniques to deepen the understanding of the microstructure and composition of materials (e.g.

iridium oxide films, nanoporous gold/oxide) used to enhance microelectrodes [29–31].

In our work, we inspect the cross section and surface of electrodeposited PtIr using SEM and scanning transmission electron microscopy (STEM) to perform a high resolution EDS (energy dispersive spectroscopy). A focused ion beam (FIB) cut was used to expose a cross section of the coating film to assess consistency and the uniformity of the coating. Carbon fiber (CF) electrodes are used as the platform for electrodeposition of PtIr. CF are an emerging technology for neural interfacing that have demonstrated excellent biocompatibility due to small cross sectional area [32]. Here, we assess the electrochemical properties and longevity of the PtIr films deposited on carbon fibers (PtIr-CF) under conditions of long-term soak testing.

2. Materials and methods

2.1. CFs microelectrode arrays fabrication

Printed circuit board (PCB) with 8 CF of ∼6.8 μm of diameter were fabricated as described in Patel *et al* [33, 34]. CF were coated with a parylene-C insulation layer (∼800 nm).

Two distinct PCB designs were used:

(a) a wide board (WB) design with eight fibers with a pitch of 2 mm and fiber length of 5 mm;
(b) a smaller PCB (ZIF Probe, ZIF), designed for *in vivo* neuronal recordings [34], with eight fibers with a pitch of 150 μm and fiber length of 2 mm.

WBs were used both for deposition process development and to produce coatings for materials analysis ($N = 71$ CF). In addition, WBs were used for soak testing due to ease of handling. A ZIF probe with 6 CF was used for the deposition process and for cross sectional analysis as will be described in the following sections.

Based on our results with the CF arrays described above, we also deposited PtIr on a small number of CF made with an alternative tip preparation process using a blowtorch to produce a sharpened CF tip [35]. The ZIF board has eight fibers (pitch of 150 μm and fiber length of 2 mm) and the tip sharpening process exposed ∼100 μm of carbon.

2.2. Pt–Ir electrochemical deposition protocol

PtIr coatings were electrodeposited using a potential cycling technique in a solution of 0.2 g l^{-1} of $Na_3IrCl_6H_2O$ and 0.186 g l^{-1} of $Na_2PtCl_6H_2O$ in 0.1 M of nitric acid (HNO_3), as previously described in Lee *et al* [26]. The solution was boiled until the color become reddish and then cooled down to room temperature. A PtIr wire electrode (∼70 μm) was used as counter and an Ag/AgCl as reference electrode (3 M NaCl, BASi, West Lafayette, IN, USA). A continuous sonication at a power of 2 W was used to improve the coating rate at initial solution temperature of 42 °C. The potential range for the electrodeposition process was −0.1 to 0.1 V with 200 mV s^{-1} of scan rate for 600 cycles, which corresponds to a coating process time of 22 min. A Gamry 600+ potentiostat was used to apply potential cycles. A Qsonica A700 (Qsonica L.L.C. Newtown, CT, USA) sonicator was used for sonication.

2.3. Electrochemical impedance spectroscopy

Electrochemical impedance spectroscopy (EIS) was collected by applying 10 mV RMS sine wave in a frequency range of 1 MHz–10 Hz. All EIS measurements were performed in 0.01 M phosphate buffered saline (PBS) solution in a three electrode configuration at open circuit potential using a stainless steel electrode as counter and an Ag/AgCl as reference electrode (3 M NaCl, BASi, West Lafayette, IN, USA). A Gamry 600+ potentiostat (Gamry Inc. Warminster, PA, USA) was used for measurement collection.

2.4. SEM and images acquisition

SEM was used to image CFs. Tescan Rise SEM (Tescan Orsay Holding, Brno—Kohoutovice, Czech Republic) was used for the acquisition of SEM images in low vacuum mode (LVSTD, low vacuum secondary electron Tescan detector) with an excitation voltage between 5 and 20 kV. This mode allows imaging without deposition of a conductive film, which is needed for pre-coating imaging due to the charging artifact of bare carbon. Chemical analysis was done using EDS with an excitation voltage of 20 kV, which allowed discrimination between the platinum and iridium molecules despite their similar energy level properties.

To analyze the cross section of the PtIr coating, a FIB was used to cut through the PtIr coating and carbon core, done on the Nova Nanolab 200 DualBeam SEM (FEI, Hillsboro, Oregon). The cut required the application of Au coating to the fibers to reduce charging. A layer of Pt was deposited on the side of the fiber in the direction of the ion bombardment to protect the surface from the cutting process. An excitation voltage of 30 kV and a current of 0.3 nA were used.

EDS analysis was also performed in STEM mode using the FEI Helios 650 Nanolab SEM/FIB after thinning the sample up to 30 nm. With this mode, the beam is finely focused and scans the sample area (as an SEM), while the image is generated by the transmitted electrons (like TEM), in this way a higher resolution power is obtained, and a more accurate EDS can be collected.

2.5. Accelerated soak test

Accelerated soak testing was done following the process used by Welle *et al* [32] to test the PtIr coated CF. In summary, EIS measurements were taken before

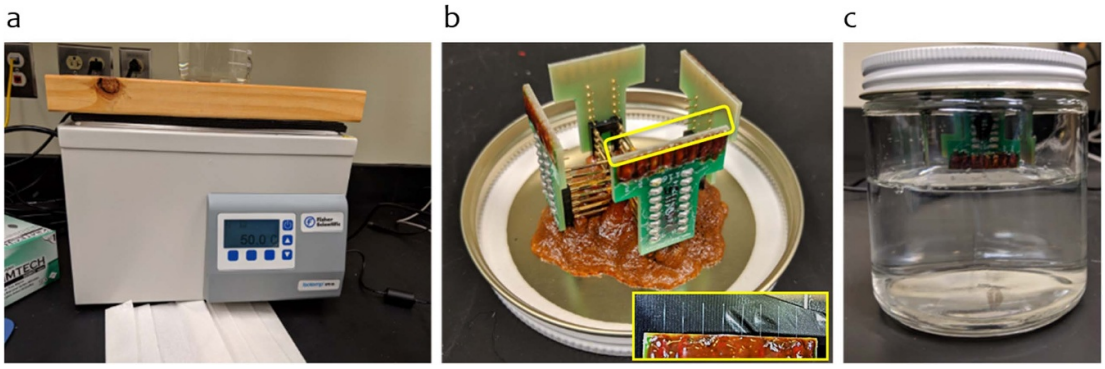

Figure 1. Soak test setup. (a) Thermo Fisher water bath set to 50 °C. (b) Soak test jar lid with the four WBs attached (the yellow box inset shows CFs, with higher magnification, on the edge of the WB). (c) Soak test jar filled with 0.01 M PBS and four attached WBs. CFs are submerged into the PBS solution by 2–3 mm.

starting the soak test and each day for the first 10 days, every 2 days from day 10 to day 20, and every 4 days until the completion of the soak test (day 36). For day 5 and day 12 we were unable to perform the EIS measurements. For the setup, four WBs were glued, using insulating epoxy (353ND, Epoxy Technology, Inc. Billerica, MA) to the bottom of the lid of two glass jars (using a 16-pin DIP socket (figure 1). Each jar contained 0.01 M PBS to a level such that the fibers were submerged about 2–3 millimeters into the solution, but the PCB was not submerged. Jars were placed in a water bath set to 50 °C. Each jar contained one control WB with bare CF (no insulation layers and no PtIr coating). WBs were removed from the soak jars and rinsed with DI water for EIS measurements. At this time, fresh PBS was placed in the soak jars. Equivalent soak time at body temperature was determined by the equation below [32, 33]:

$$t_{37} = t_T \times Q10^{(T-37)/10} \quad (1)$$

in which $\mathbf{t_{37}}$ is the simulated aging time at 37 °C, $\mathbf{t_T}$ is the amount of actual soak time at $T = 50$ °C, and Q10 is an aging factor that is equal to 2.283 according to ASTM guidelines for polymer aging [36]. Calculating the simulated time for $\mathbf{t_T} = 1$, the accelerating factor $\mathbf{t_{37}}$ is equal to 2.46 and all real time measurements are scaled by this amount to obtain the simulated time. In our case the simulated time is 89 days.

The test structure used (WB) is designed for rapid and economical assembly, at the expense of yield and robustness. Thus, we noted (during soak test) failures consistent with open circuits, which were characterized by 1 kHz impedance exceeding 1 MOhm and a capacitive impedance spectrum. This impedance change was noted when fibers were visibly missing, but also with fibers that appear intact (including PtIr remaining on the CF). The latter we attributed to an internal fault in the bonding. Open circuits were not included in the impedance data analysis (see section 3.4). For the control bare CF (see section 3.4), we noted a sudden increase in impedance on the last day of testing, with multiple CF measuring above 500 kOhm, where none had measured above this level on any prior day. We excluded this last day of measurements from the control bare CF data analysis.

2.6. Equivalent circuit model and statistical analysis

To analyze impedance data before and after the PtIr coating, an equivalent circuit model was fitted using the Gamry Echem Analyst software. The circuit model is shown in the inset of figure 2(a). The model components are defined as follows: Ru—electrolyte resistance, C—parasitic capacitance, Y0—the admittance of the constant phase element (CPE), α exponent of the CPE, r.e.—reference electrode, w.e.—working electrode. Impedance data were fitted for CF, PtIr-CF, and overcoated PtIr-CF (see results sections 3.1 and 3.2). Model components values extracted from fitting were compared using a paired t-test for comparison of CF to CF-PtIr. Since CF-PtIr and overcoated PtIr-CF had different sample sizes, a two-sample t-test was used. In both cases, significance was set at $p = 0.05$. Impedance (@ 1 kHz) of CF and PtIr-CF were compared using a paired t-test with significance difference at 0.05. The mean impedance trends (@ 1 kHz and @100 kHz) during soak testing were analyzed using a linear regression model for which the trend-lines and the statistic coefficients (p-value, slope, R^2 and R) were computed. Matlab version 2018b (Mathworks, Natick, MA, USA) was used both for the paired t-test, the two sample t-test and for the linear regression analysis.

3. Results

3.1. PtIr Coating process development

A total of 77 CF on 16 WBs and 1 ZIF were coated with PtIr. EIS measurements were collected prior to and after PtIr coating. EIS magnitude consistently decreased after the coating process, with a mean impedance magnitude ($N = 70$ coated CF) decrease

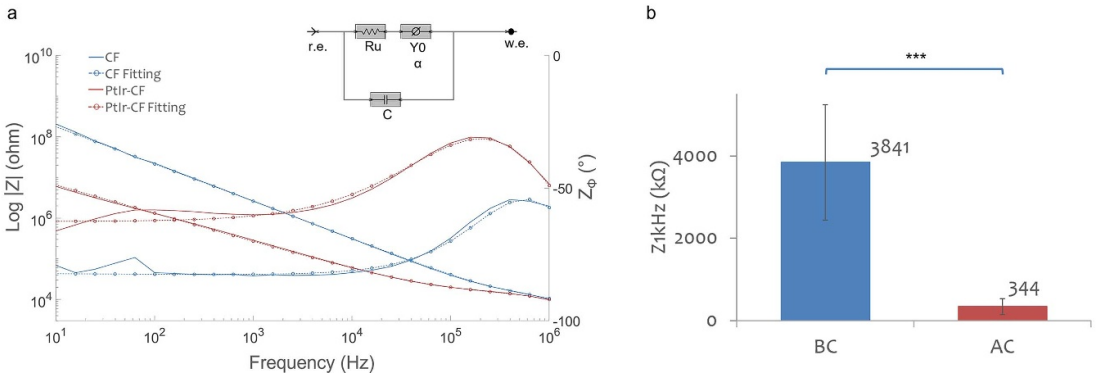

Figure 2. EIS measurements of PtIr-CF. (a) Magnitude impedance trend of one PtIr-CF is reported before (solid blue line) and after the coating process (solid red line). As inset the equivalent circuit model used to fit impedance data is reported; fitted impedance magnitude and phase as reported before (blue dashed line) and after the coating (red dashed lines). (b) Mean and standard deviation of impedance @ 1 kHz before (blue) and after (red) the coating ($N = 70$ CF); the *** indicates a p-value $= 9.37 \times 10^{-7}$.

Table 1. List of all component extracted from the equivalent circuit model shown in figure 2(a) for CF and PtIr-CF. The p-value from the paired t-test are reported with a significance difference for the CPE components.

	Ru	Y0	α	C
CF	$3.06 \pm 5.4 \times 10^{4}$	$1.43 \pm 1.26 \times 10^{-10}$	0.86 ± 0.08	$8.09 \pm 3.6 \times 10^{-12}$
PtIr-CF	$2.8 \pm 5.4 \times 10^{4}$	$1 \pm 1.64 \times 10^{-8}$	0.71 ± 0.06	$1.55 \pm 4.7 \times 10^{-11}$
p-value	0.74	4.4×10^{-6}	7.6×10^{-21}	0.2

of 89% ± 4.9% @ 1 kHz (mean ± standard deviation). We excluded 7 PtIr-CF due to overcoating. An example of the EIS measurement of a CF and PtIr-CF is shown in figure 2(a), blue and red solid lines respectively. The impedance trend were fitted to an equivalent circuit model (inset of figure 2(a)) and the fitted lines are reported as red and dashed blue lines for CF and PtIr-CF respectively. The fitting was done for all 70 CF and PtIr-CF. The mean values of the extracted circuit parameters (Ru, Y0, α, C) are reported in table 1 with the standard deviation and the p-values from the paired t-test. The higher value of the admittance (Y0) of the CPE confirms a lower electrode impedance for the PtIr-CF. The difference between the admittance and the α value of CF and PtIr-CF was statistically significant.

In figure 2(b) the mean impedance @ 1 kHz ($N =$ 70 coated CF) before and after PtIr coating is reported with standard deviation. The difference in impedance @ 1 kHz was statistically significant (paired t-test, p-value $= 9.37 \times 10^{-7}$).

To study the PtIr coating morphology on the CF surface, SEM images were collected. PtIr coating was observed on most part of the active electrode surface of a PtIr-CF (figure 3(a)), with some bare areas (yellow arrow). To quantify the PtIr percentage composition, an energy dispersive x-ray spectroscopy map was collected and the percentage of Pt and Ir was calculated on the PtIr-CF surface. From the spectra (figure 3(b)) collected with the EDS map, Pt and Ir peaks can be distinguished at 9 keV corresponding to a percentage of 74% and 26% of Pt and Ir respectively.

3.2. OverCoated PtIr-CF

Out of 77 PtIr-CF, 7 appeared overcoated, meaning that PtIr was deposited outside the carbon electrode area and over the parylene-C insulated fiber, effectively increasing the geometric surface area. The impedance data of the overcoated CF ($N = 7$) were fitted to the equivalent circuit of figure 2(a). The mean values of the extracted parameters (Ru $= 9.10 \pm 2 \times 10^{3}$, Y0 $= 1.47 \pm 0.81 \times 10^{-08}$, $\alpha = 0.72 \pm 0.01$, $C = 1.03 \pm 0.069 \times 10^{-11}$) were not statistically significant with the respect to the PtIr-CF that did not appear overcoated ($N = 70$), with the exception of Ru (two sample t-test, $p_{Ru} = 0.006$, $p_{Y0} = 0.3$, $p_{\alpha} = 0.12$, $p_{C} = 0.35$). The lower Ru with the respect to regular PtIr-CF suggest a lower impedance at high frequency which indicates an increased electrode geometric area.

3.3. PtIr cross-sectional analysis

A FIB cut of an overcoated probe was performed to inspect both the carbon-PtIr interface and the region of overcoating (carbon-parylene-PtIr interface). In figure 4(a) the SEM image of the PtIr-CF before the FIB cut is shown, with the yellow rectangular cutting pattern highlighted.

The PtIr coating was found to be mostly continuous (figure 4(b)) with some voids as shown on the CF tip (figure 4(c), green box, red arrows) and an average PtIr coating thickness of 418.7 ± 86 nm along the fiber surface (11 measured areas). This thickness is consistent with other earlier reports of PtIr [37]. In figure 4(c) (green box) some PtIr deposits appear

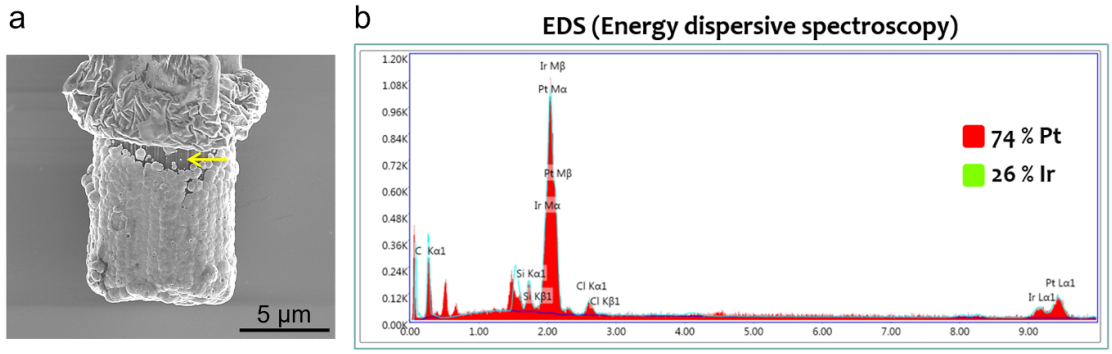

Figure 3. SEM image and EDS measurement of PtIr-CF. (a) SEM image of one PtIr-CF showing the insulation parylene-C layer and the PtIr coating deposited on the CF electrode site (yellow arrow indicating CF bare area). (b) Chemical spectra from the EDS map on the CF active surface showing the two different peaks associated to Pt and Ir at 9 keV.

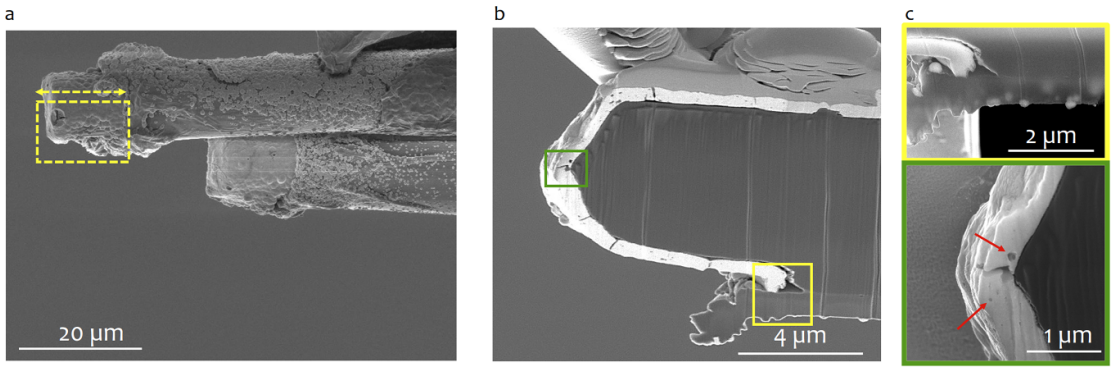

Figure 4. FIB cut of PtIr-CF. (a) SEM image of the overcoated CF showing the yellow rectangle pattern cut. (b) SEM images of the cut intersection with two pattern highlighting the tip (green) with visible voids ((c), green box, red arrows) and the parylene-C insulation layer (yellow) showing embedded PtIr molecules at high resolution ((c), yellow box).

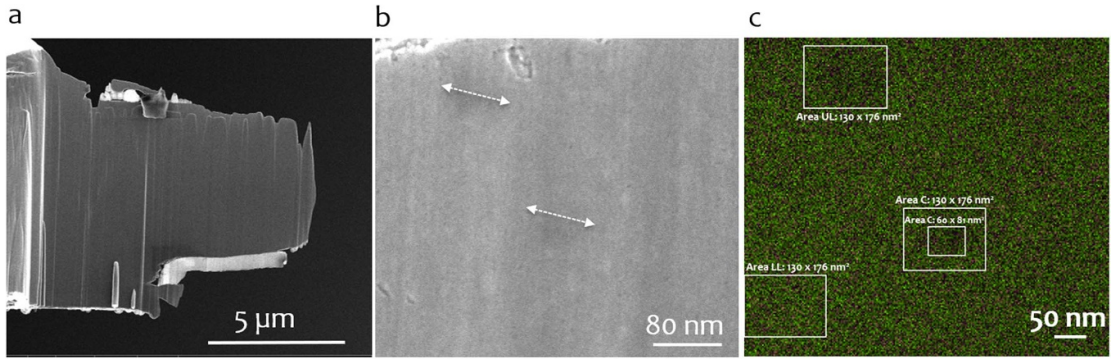

Figure 5. SEM imaging of the CF—PtIr coating intersection. (a) SEM image of the CF and PtIr intersection after sample thinning. Some PtIr coating was lost during the thinning process. (b) Magnified SEM image of a cross section of the coating with white arrow highlighted two dark regions. (c) EDS (at 25 keV) of the coated area showing the Pt and Ir molecules, respectively, in green and light pink, with callipers showing regions of interest that were examined quantitatively.

to be embedded into the parylene-C insulation layer, which suggests a mechanism for overcoating noted earlier.

To inspect the PtIr coating with higher resolution, a PtIr-CF was thinned to ∼30 nm (In figure 5(a)). Given that the sample area is placed immediately under the detector in STEM mode, a thinner sample is necessary in order to achieve a high-resolution EDS, but the thinning process results in some missing material due to sample preparation. In figure 5(b) the chosen region of the PtIr coating for EDS is shown and darker areas can be noticed within the PtIr that may suggest different PtIr density (figure 5(b) white arrows) as also appeared in TEM analysis where dark and bright molecules aggregates were appreciated (data not shown).

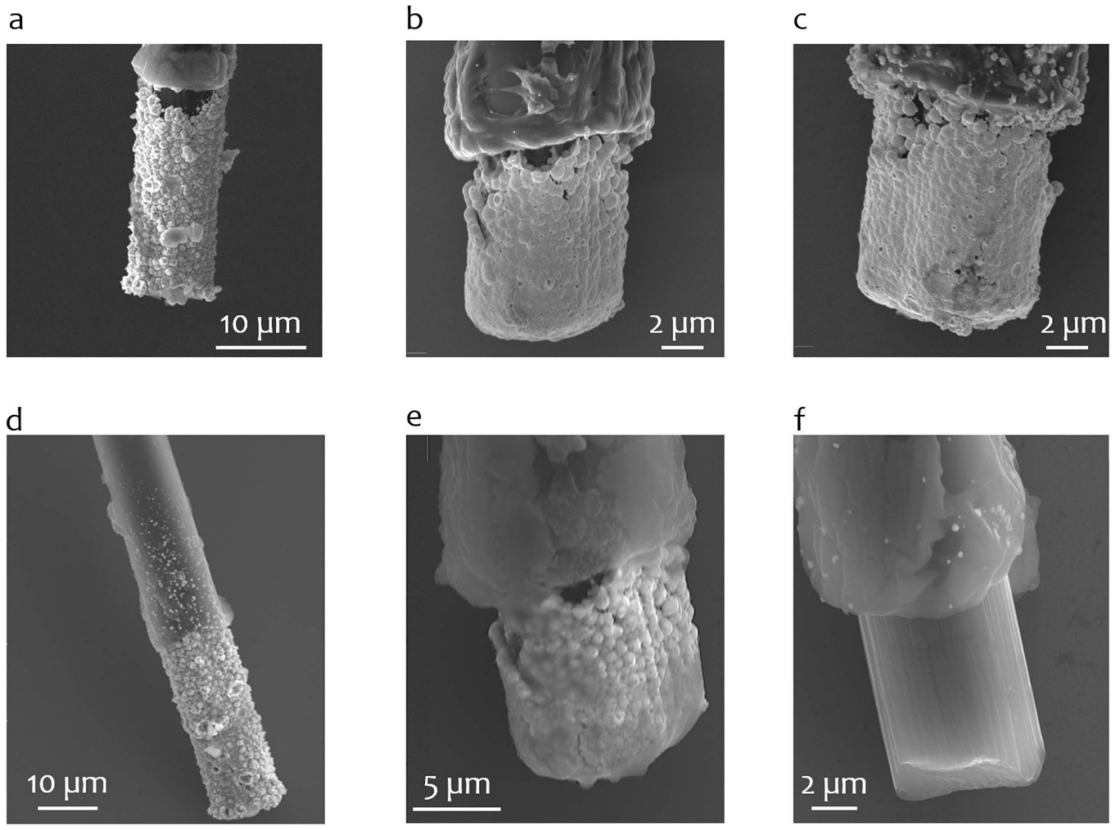

Figure 6. SEM of soak tested PtIr-CF. PtIr-CF before (upper panel: (a)–(c)) and after (lower panel: (d)–(f)) 36 days of soak testing. Comparing (b)–(e) shows evidence of a crack in the film after soaking in this case, but not significant loss of material.

EDS mapping of the entire region yields 72% and 28% of Pt and Ir respectively (figure 5(c)). To assess the significance of bright and dark regions noticed in the PtIr coating EDS maps have been collected in four regions of interests (figure 5(c)). The average percentage values of Pt and Ir for the four analyzed areas (three of 130×176 nm^2 and one of 60×81 nm^2) was $70.5 \pm 2.3\%$ for Pt and 29.5 ± 2.38 for % Ir. In addition, an EDS spectrum of the dark spots overlaid with a closer brighter area (data not shown) confirmed that the different appearance was due to different thickness of the sample in distinct areas and not to different material composition.

3.4. Soak test

Heated soak test was performed on 59 CFs for 36 days (six WB with $N = 43$ PtIr-CF and 2 WB with $N = 16$ bare control CF). SEM images were collected for all CF before and after the soak test. A representative panel of PtIr-CF before (upper panel, a–c) and after (lower panel d–f) the soak test is shown in figure 6. Out of 43 PtIr-CF that underwent soak testing, two were mechanically broken (the fiber was not attached anymore to the PCB). Of the remaining 41 CF-PtIr samples examined after the soak test, 33 showed no obvious changes in appearance (represented by figures 6(a) and (d)), three showed insulation layer covering the coated area (data not shown), three showed loss of PtIr coating (figures 6(c) and (f)) and two showed evidence of cracking (figures 6(b) and (e)). Residue was observed on 16 CF (both PtIr-CF and control CF). EDS analysis on three PtIr-CF confirmed that the residue was NaCl (see figure 6(e)).

Regular impedance testing revealed that 16 PtIr-CF were electrically disconnected within the first 10 days of soak test, based on a capacitive impedance spectrum consistent with an open circuit. Although the PtIr coating remained adherent, impedance could not be measured on these PtIr-CF due to the open circuit. These 16 samples, the three that lost PtIr plus the three that had insulation covering the coated area were removed from the long-term impedance analysis.

We performed a statistical analysis considering the 19 PtIr-CF that had complete impedance data. The mean impedance and standard deviation @ 1 and 100 kHz is reported in figures 7(a) and (b). An increase of 12% and 13% was detected after 36 days of the soak test respect to day 0 @1 and @100 kHz, respectively. We applied a linear regression model of which the trend-lines (dashed blue and red lines) and the statistic coefficients (p-value, slope, R^2 and R) are reported in figures 7(a) and (b). The correlation coefficient R of 0.7 suggest a strong correlation between the impedance variation @1 kHz and the increasing of soak testing days. The rate of change of 4 kΩ day^{-1} @1 kHz was statistically significant (p-value = 0.003). In contrast, the 100 kHz impedance did not show a

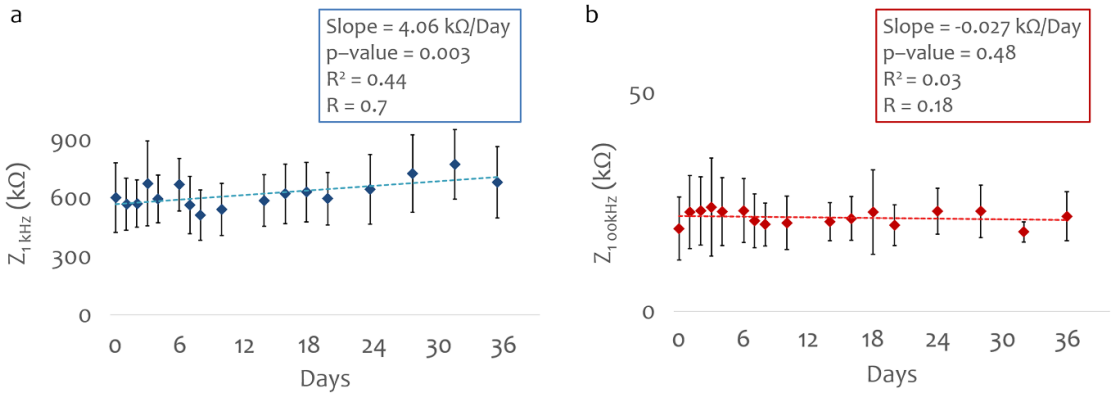

Figure 7. Average soak test impedance. (a) Mean and standard deviation of the impedance trend @ 1 kHz and (b) 100 kHz for $N = 19$ Pt-Ir CF that completed the soak test ($Z_{1kz} < 1$ MΩ from day 0 to day 36); the blue and red dashed lines represent the trend-lines of the linear regression model and the slope, the p-value, the R^2 and the correlation coefficient R are reported in the inset.

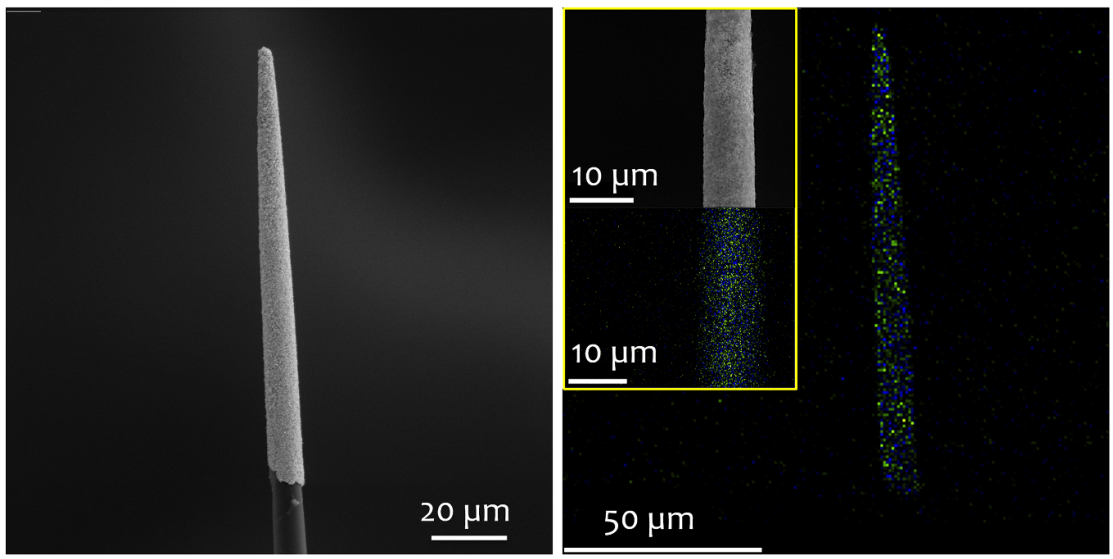

Figure 8. SEM Images of a Blowtorched PtIr-CF. (a) SEM of a sharpened CF; (b) EDS analysis of the PtIr-CF (green for Pt and blue for Ir) and of a small section (8×32 μm^2, yellow inset).

clear trend and any changes in this impedance are unrelated to days in soak test (p-value $= 0.48 > 0.05$). For the control bare CF an impedance increase of 13% @1 kHz was detected between the last (day 28th, see section 2.5) and the first day of soak testing (data not shown).

3.5. Improving coated surface coverage

Some defects were apparent in the PtIr films analyzed and tested. Figures 3(a) and 6(a)–(c) show PtIr films with gaps in coverage or cracks. Possible causes for these defects include surface contamination from incomplete cleaning before coating and plating solution contamination from degradation of the sonicator tip, the latter resulting in deposition of poorly adherent titanium chunks that later dislodge and leave behind a gap in the film.

To investigate methods to improve film uniformity and continuity of coverage, we used CFs produced by an updated manufacturing process that included more cleaning steps. The new process uses blowtorching [35] technique to sharpen the CFs tip and oxygen plasma as final cleaning step before the coating. Both blowtorching and oxygen plasma removed residual parylene from the electrode surface. The plating procedure has been modified with a higher initial temperature that is held constant during deposition as well with a pulsed sonication (instead of a continuous sonication). With these modifications, no gaps in coverage were apparent and the composition of the film was maintained at 71% Pt and 29% Pt (figure 8(b)). EDS of a small area (8×32 μm^2, yellow box in figure 8(b)) confirms the homogeneous distribution of Pt and Ir of the film (Pt = 69% and Ir = 31%)).

4. Discussion and conclusions

We have analyzed PtIr composition and showed that deposition of this alloy on CFs improves the impedance characteristics without increasing the geometric area. Analysis of the deposited PtIr film showed that platinum and iridium were evenly distributed within the film. Cross sections of the film appear generally uniform in thickness with minimal evidence of cracks and/or voids. Accelerated soak testing for a simulated 89 days (36 soak testing days) showed that the film remained adherent to 38 of 41 samples analyzed after soak testing. PtIr films tested in this study did show some undesirable properties, including cracks (figure 6(c)) and gaps in coverage (figures 3(a) and 6(a), (b)). We demonstrated a potential solution to these problems using a meticulously cleaned carbon surface and minor adjustment to our plating protocol. With these modifications, uniform tip coverage was shown and the composition of the film maintained at ∼70% Pt and 30% Ir. These findings suggest that PtIr electrodeposition is a viable option for improving the electrical properties of CFs electrodes.

Devices fabricated using the process described in this report require further validation with acute and chronic *in vivo* neural recordings. For microstimulation applications, *in vitro* and long-term *in vivo* testing, similar to what has been done with PtIr on other electrode substrates [27], will be required to extend PtIr-CF into neurostimulation applications.

The process as described is sufficiently reliable for research electrodes, although overcoating must be avoided. For a clinical device, near 100% reliability will be needed. Thus, process development, like those presented to improve coverage, must continue to further improve film consistency and durability, if PtIr-CF are to be translated to human use.

Data availability statement

All data that support the findings of this study are included within the article (and any supplementary files).

Acknowledgments

This work was financially supported by the National Science Foundation (DMR-0320740, DMR-9871177 and DMR-1625671), by the National Institutes of Health National Institute of Neurological Disorders and Stroke (U01NS094375 and UF1NS107659), the Office of the Director National Institutes of Health (OT2OD024907), the NSF-funded NeuroNex Hub MINT (Multimodal Integrated Neural Technologies) at the University of Michigan under NSF 1707316, the Kellogg Vision Research Core funded by P30 EY007003 from the National Eye Institute, The University of Michigan College of Engineering, the School of Medicine, and Research to Prevent Blindness. The authors acknowledge technical and scientific support from Julianna Richie and Dr Paras Patel from the Cortical Neural Prosthetics Lab at University of Michigan. The authors also acknowledge technical support from the Michigan Center for Materials Characterization, specifically from Mr Bobby Kerns and Dr Allen Hunter for their training and guidance. The Author J D W has a financial interest in PtIr coatings.

ORCID iDs

Elena della Valle https://orcid.org/0000-0001-8874-7982
Elissa J Welle https://orcid.org/0000-0001-5141-7656
Cynthia A Chestek https://orcid.org/0000-0002-9671-7051
James D Weiland https://orcid.org/0000-0003-3453-9074

References

[1] Amirnovin R, Williams Z M, Rees Cosgrove G and Eskandar E N 2006 Experience with microelectrode guided subthalamic nucleus deep brain stimulation *Oper. Neurosurg.* **58** ONS–96
[2] Coelli S, Levi V, Del Vecchio Del Vecchio J, Mailland E, Rinaldo S, Eleopra R and Bianchi A M 2021 An intra-operative feature-based classification of microelectrode recordings to support the subthalamic nucleus functional identification during deep brain stimulation surgery *J. Neural Eng.* **18** 016003
[3] Lima J C F V, de Carvalho M D M H and Dias J M B 2015 Analysis and classification of microelectrode recordings in deep brain stimulation surgery *Academia* 1–13
[4] Danish S F, Baltuch G H, Jaggi J L and Wong S 2008 Determination of subthalamic nucleus location by quantitative analysis of despiked background neural activity from microelectrode recordings obtained during deep brain stimulation surgery *J. Clin. Neurophysiol.* **25** 98–103
[5] Parastarfeizabadi M and Kouzani A Z 2017 Advances in closed-loop deep brain stimulation devices *J. Neuroeng. Rehabil.* **14** 1–20
[6] Markert M S and Fisher R S 2019 Neuromodulation-science and practice in epilepsy: vagus nerve stimulation, thalamic deep brain stimulation and responsive neurostimulation *Expert Rev. Neurother.* **19** 17–29
[7] Enhui H, Shengwei X, Xiao G, Dai Y, Xinrong Li, Song Y, Gao F, Zhang Y, Xu S and Cai X 2021 MWCNTs/PEDOT: PSS nanocomposites-modified microelectrode array for spatial dynamics recording of epileptic discharges in multi-subregion of hippocampal slice *Sens. Actuators* B **329** 129190
[8] Xiao G, Song Y, Zhang Y, Xing Y, Xu S, Lu Z, Wang M and Cai X 2020 Cellular-scale microelectrode arrays to monitor movement-related neuron activities in the epileptic hippocampus of awake mice *IEEE Trans. Biomed. Eng.* **68** 19–25
[9] Lu C W, Malaga K A, Chou K L, Chestek C A and Patil P G 2020 High density microelectrode recording predicts span of therapeutic tissue activation volumes in subthalamic deep brain stimulation for parkinson disease *Brain Stimul.* **13** 412–19
[10] Nigam A, Ahmed F and Pawar S J 2020 Design and simulation of geometrical shape and size variations of

micro-electrode for cochlear implant *Biotechnological Applications in Human Health* (Berlin: Springer) pp 69–75
[11] Jian W, Yan L, Xu H, Tang W C and Zeng F-G 2005 A curvature-controlled 3D micro-electrode array for cochlear implants *The 13th Int. Conf. on Solid-State Sensors, Actuators and Microsystems, 2005 Digest of Technical Papers. TRANSDUCERS'05* vol 2 (IEEE) pp 1636–9
[12] Weiland J D, Liu W and Humayun M S 2005 Retinal prosthesis *Annu. Rev. Biomed. Eng.* **7** 361–401
[13] Lyu Q *et al* 2020 A three-dimensional microelectrode array to generate virtual electrodes for epiretinal prosthesis based on a modeling study *Int. J. Neural Syst.* **30** 2050006
[14] Zhou D D and Greenberg R J 2009 Microelectronic visual prostheses *Implantable Neural Prostheses 1. Biological and Medical Physics, Biomedical Engineering* ed E Greenbaum and D EZhou (Berlin: Springer) p 1–42
[15] Ryu S B, Werginz P and Fried S I 2019 Response of mouse visual cortical neurons to electric stimulation of the retina *Front. Neurosci.* **13** 324
[16] Schwartz A B 2004 Cortical neural prosthetics *Annu. Rev. Neurosci.* **27** 487–507
[17] Buzsáki G 2004 Large-scale recording of neuronal ensembles *Nat. Neurosci.* **7** 446–51
[18] Lebedev M A and Nicolelis M A L 2017 Brain-machine interfaces: from basic science to neuroprostheses and neurorehabilitation *Physiol. Rev.* **97** 767–837
[19] Chen X, Wang F, Fernandez E and Roelfsema P R 2020 Shape perception via a high-channel-count neuroprosthesis in monkey visual cortex *Science* **370** 1191–6
[20] Zheng X S, Tan C, Castagnola E and Cui X T 2021 Electrode materials for chronic electrical microstimulation *Adv. Healthcare Mater.* **10** 2100119
[21] Klein J D, Clauson S L and Cogan S F 1989 Morphology and charge capacity of sputtered iridium oxide films *J. Vac. Sci. Technol.* A **7** 3043–7
[22] Beebe X and Rose T L 1988 Charge injection limits of activated iridium oxide electrodes with 0.2 ms pulses in bicarbonate buffered saline (neurological stimulation application) *IEEE Trans. Biomed. Eng.* **35** 494–5
[23] Cogan S F 2008 Neural stimulation and recording electrodes *Annu. Rev. Biomed. Eng.* **10** 275–309
[24] Fan B, Rodriguez A V, Vercosa D G, Kemere C and Robinson J T 2020 Sputtered porous Pt for wafer-scale manufacture of low-impedance flexible microelectrodes *J. Neural Eng.* **17** 036029
[25] Elyahoodayan S, Jiang W, Lee C D, Shao X, Weiland G, Whalen Iii J J, Petrossians A and Song D 2021 Stimulation and recording of the hippocampus using the same Pt-Ir coated microelectrodes *Front. Neurosci.* **15** 137
[26] Lee C D, Hudak E M, Whalen III J J, Petrossians A and Weiland J D 2018 Low-impedance, high surface area Pt-Ir electrodeposited on cochlear implant electrodes *J. Electrochem. Soc.* **165** G3015
[27] Cassar I R, Chunxiu Y, Sambangi J, Lee C D, Whalen III J J, Petrossians A and Grill W M 2019 Electrodeposited platinum-iridium coating improves *in vivo* recording performance of chronically implanted microelectrode arrays *Biomaterials* **205** 120–32
[28] Sarno M, Ponticorvo E and Scarpa D 2019 Controlled PtIr nanoalloy as an electro-oxidation platform for methanol reaction and ammonia detection *Nanotechnology* **30** 394004
[29] Lee I-S, Whang C-N, Lee Y-H, Lee G H, Park B-J, Park J-C, Seo W-S and Cui F-Z 2005 Formation of nano iridium oxide: material properties and neural cell culture *Thin Solid Films* **475** 332–6
[30] Sachse R, Hertwig A, Kraehnert R and Hodoroaba V-D 2018 Analysis of mesoporous iridium oxide thin films by the combined methodical approach SEM/EDS/STRATAGem *Microsc. Microanal.* **24** 762–3
[31] Kim Y H, Kim G H, Kim M S and Jung S-D 2016 Iridium oxide–electrodeposited nanoporous gold multielectrode array with enhanced stimulus efficacy *Nano Lett.* **16** 7163–8
[32] Welle E J *et al* 2020 Ultra-small carbon fiber electrode recording site optimization and improved *in vivo* chronic recording yield *J. Neural Eng.* **17** 026037
[33] Patel P R, Kyounghwan N, Zhang H, Kozai T D Y, Kotov N A, Yoon E and Chestek C A 2015 Insertion of linear 8.4 μm diameter 16 channel carbon fiber electrode arrays for single unit recordings *J. Neural Eng.* **12** 046009
[34] Patel P R, Zhang H, Robbins M T, Nofar J B, Marshall S P, Kobylarek M J, Kozai T D Y, Kotov N A and Chestek C A 2016 Chronic *in vivo* stability assessment of carbon fiber microelectrode arrays *J. Neural Eng.* **13** 066002
[35] Welle E J, Woods J E, Jiman A A, Richie J M, Bottorff E C, Ouyang Z, Seymour J P, Patel P R, Bruns T M and Chestek C A 2021 Sharpened and mechanically robust carbon fiber electrode arrays for neural interfacing *bioRxiv* (https://doi.org/10.1101/2021.01.21.427697)
[36] ASTM A 2016 Standard guide for accelerated aging of sterile barrier systems for medical devices. *ASTM Int. West Conshohoken, PA, USA* 2016
[37] Petrossians A, Whalen III J J, Weiland J D and Mansfeld F 2011 Electrodeposition and characterization of thin-film platinum-iridium alloys for biological interfaces *J. Electrochem. Soc.* **158** D269